Lab on a Chip

Micro- & nano- fluidic research for chemistry, physics, biology, & bioengineering

www.rsc.org/loc

Volume 10 | Number 7 | 7 April 2010 | Pages 801–924

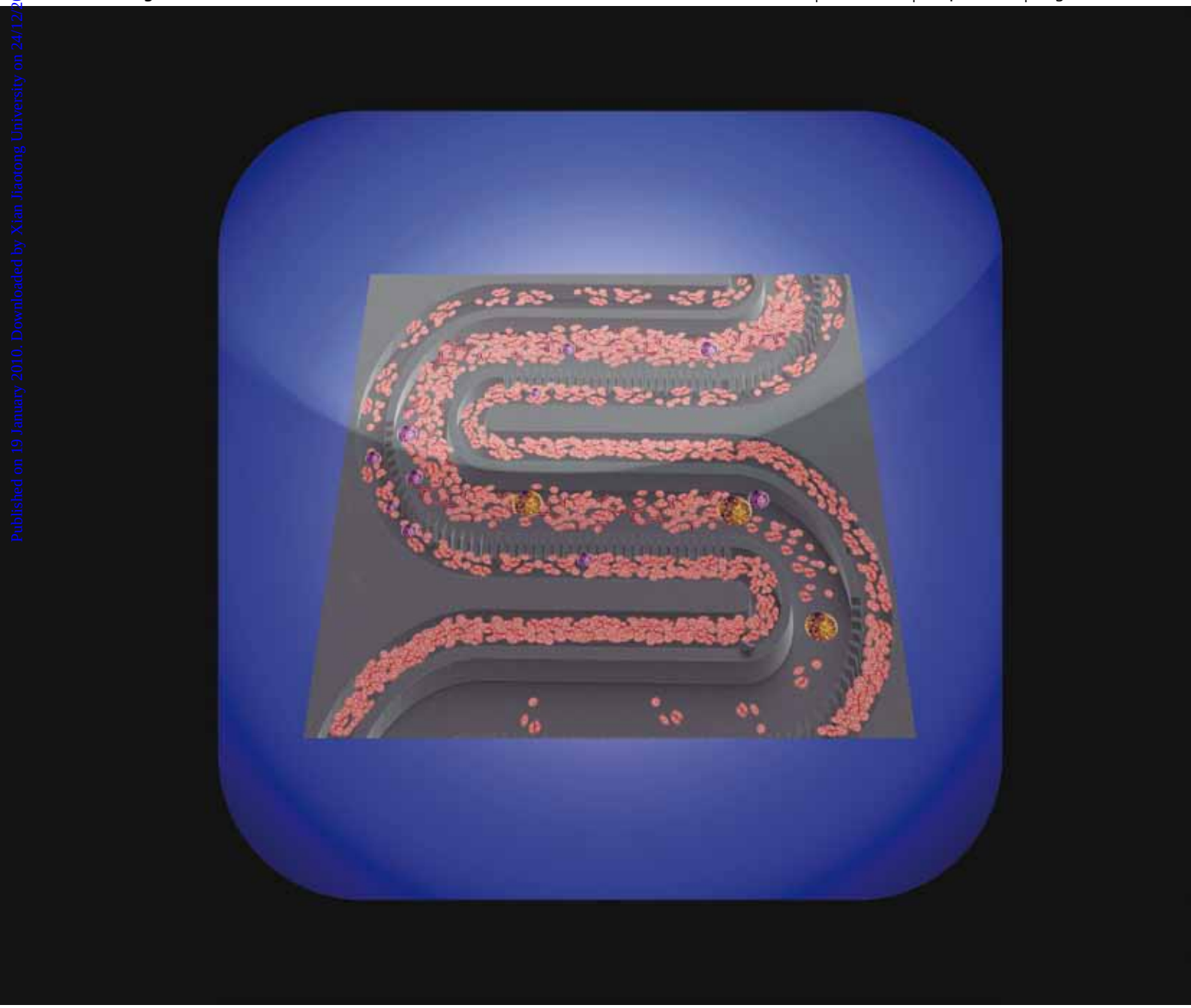

ISSN 1473-0197

RSC Publishing

Chiu
Filtration biophysics

Schonbrun
200 000 drops s^{-1} detection

Madou
Modelling microchamber filling

Allbritton
Air-stable membranes

Deformability considerations in filtration of biological cells†

Jason S. Kuo, Yongxi Zhao, Perry G. Schiro, Laiying Ng, David S. W. Lim, J. Patrick Shelby and Daniel T. Chiu*

Received 27th October 2009, Accepted 16th December 2009
First published as an Advance Article on the web 19th January 2010
DOI: 10.1039/b922301k

Biological cells are highly sensitive to variation in local pressure because cellular membranes are not rigid. Unlike microbeads, cells deform under pressure or even lyse. In isolating or enriching cells by mechanical filtration, pressure-induced lysis is exacerbated when high local fluidic velocity is present or when a filter reaches its intended capacity. Microfabrication offers new possibilities to design fluidic environments to reduce cellular stress during the filtration process. We describe the underlying biophysics of cellular stress and general solutions to scale up filtration processes for biological cells.

Introduction

Rare cells, which include circulating tumor cells (CTC) in peripheral blood,[1–8] fetal cells in maternal blood,[9–14] and cancer stem cells[15–18] are difficult to isolate consistently. Often present at concentrations approaching the stochastic noise level, rare cells are notoriously vulnerable to inadvertent losses during the cell separation process. Frequent culprits of losses can include, for example, antibody-labeling efficiency, chemical or mechanical damage (*e.g.* lysis), and transfer losses (*e.g.* cell adhesion in tubings, centrifuge tubes, or other contacting surfaces). Sources of losses must be systematically examined to reduce the rate of false-negatives.

This paper focuses on the mechanism of cellular damage in a filtration environment in the context of CTC isolation from peripheral blood. Filtration as a viable method to isolate tumor cells from peripheral blood was first discussed by S. H. Seal in 1964 in the development of a plastic sieve produced by charged-particle bombardment followed by etching ("track-etched").[19] Shortly thereafter R. L. Fleisher *et al.* demonstrated the utility of such a sieve to isolate cancer cells in a proof-of-concept experiment.[20] Recently similar sieves were used in clinical analysis of patient specimens: Paterlini-Brechot and co-workers[5,14,21–23] used a polycarbonate microparticulate filter (with randomly arranged 8 μm pores) in a custom-designed housing to isolate cancer cells from the peripheral blood of cancer patients. The filter housing allowed convenient removal of the filter membrane, which was then placed directly on a microscope for cell enumeration. The resulting CTC count was successfully correlated to the clinical outcomes of patients with liver cancer[22] and breast cancer.[24,25]

With advances in microfabrication, filter pore geometry and the spatial arrangement of pores could be designed and produced with precision. For example, to address throughput needs, Zheng *et al.*[7] produced a planar parylene membrane filter with a high density of circular or oval pores (16 000 pores in an area of 0.6 cm × 0.6 cm) for isolating tumor cells from spiked blood samples. Recently Tan *et al.*[26] developed a PDMS-based microdevice with multiple arrays of crescent-shaped isolation wells to isolate cancer cells from spiked blood. The isolation wells contained gaps of 5 μm to allow flow-through of erythrocytes and deformable leucocytes.

We describe in this paper the underlying biophysics of filtration, with emphasis on the pressure experienced by cells under various hydrodynamic environments that could lead to inadvertent deformation and lysis. We also report a filtration chip that is simple in construction yet offers isolation and concentration of CTCs into a small collection area for fast inspection by clinical personnel.

Experimental

Filtration design

Fig. 1 illustrates the layout of a filtration chip that we developed and the images of select regions of the chip. Whole human blood was introduced into the inlet of the chip (Fig. 1(B)), which consisted of a serpentine channel (100 μm (W) × ~45 μm (H), scanning electron microscopy image shown in Fig. 1(A)) lined with tall rectangular apertures (8 μm (W) × 45 μm (H)) connecting to two outer filtrate channels. We term these apertures one-dimensional ("1-D") apertures to denote that these apertures are larger than the cancer cells they are intended to exclude in at least one dimension, as opposed to zero-dimensional ("0-D") apertures which are smaller than the cells these apertures exclude. Small circular pores, such as those commonly found in track-etched filters, are examples of 0-D apertures as they can be completely sealed by the cells they are intended to exclude. These 1-D apertures retained cancer cells within the main flow channel but allowed erythrocytes and majority of leucocytes to cross into the filtrate channels (Fig. 1(B), magnified views). The retained cancer cells were forced to flow along the serpentine channel to the outlet, where they were concentrated and collected by a final set of 1-D apertures. Unlike a classic tangential-flow configuration, in this design no fluid is allowed to exit without crossing an aperture.

To prevent back-flowing of filtrate from the outer channels into the main serpentine channel as the fluid path curved along the U-bends, 1-D apertures were replaced with baffles or solid

Department of Chemistry, University of Washington, Seattle, WA, 98195-1700, USA. E-mail: chiu@chem.washington.edu; Fax: +1 206 685 8665; Tel: +1 206 543 1655

† Electronic supplementary information (ESI) available: Movie of leucocytes lodged at 1-D apertures. See DOI: 10.1039/b922301k

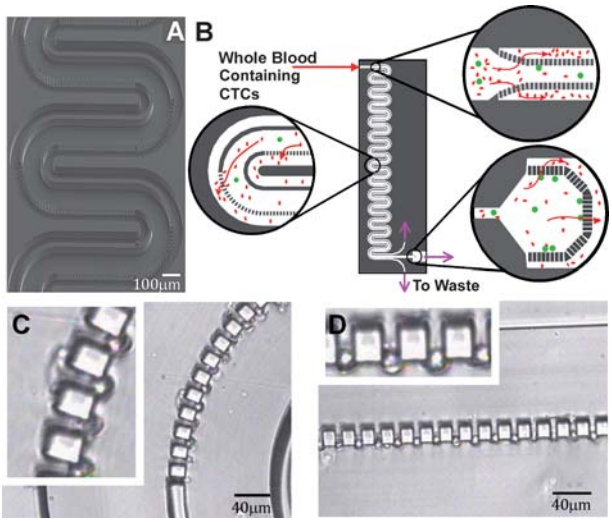

Fig. 1 Schematic and images showing the operation of a CTC-isolation biochip. **(A)** SEM image of the serpentine section of the chip. **(B)** Layout of the biochip: whole blood enters from the upper left, encounters a filtration section that consists of 1-D apertures on two sides of the main flow channel. The filtration section becomes a long serpentine channel, and enters into a trap area at the end of the serpentine. Magnified illustrations are not drawn to scale. **(C)** Microscopy images taken during flow of diluted (healthy) human blood showing leucocytes trapped at the entrances of 1-D apertures at a turn of the serpentine channel. Inset is the enlarged view. **(D)** Additional images of leucocytes trapped in flow in a straight section of the serpentine.

walls at select locations as fluid changed direction. Because the outer edge of each bend was lined with 1-D apertures, some component of the fluidic momentum—in particular the velocity component normal to the apertures—"leaked" through these apertures, resulting in an overall reduction of the fluidic momentum in the main serpentine channel as fluid exited each bend.

Fig. 1(C) and 1(D) show bright-field images of the chip in operation. Diluted whole human blood from healthy donors was flowed though the chip. In general individual blood cells were traveling too fast to be seen by the naked eye except those, typically the larger leucocytes, trapped near the 1-D apertures (insets of Fig. 1(C) and 1(D)). We observed that in some instances the trapped leucocytes were rotating rapidly due to a delicate force-balance between the tangential shear of the flow in the main channel and that of the flow bypassing the cells and entering the 1-D apertures (see the movie in the ESI†). Free rotation suggested that cells could be captured without being in hard mechanical contact with (*i.e.* pinned against) the microstructures.

Upon exiting the serpentine the rare cells were intercepted by a final set of 1-D apertures distributed across the flow path. At this exit the channel cross-section was enlarged with a cone by 10 times to reduce the velocity directly impinging on the normal apertures. Nominally, at 25 μL min^{-1} fluidic throughput, the velocity entering the filtration serpentine was ~3 cm s^{-1}. Exiting the cone the velocity would have reduced to ~0.3 cm s^{-1}, assuming no momentum was lost in the serpentine. This is an upper estimate since momentum was continuously lost into the filtrate channels at each U-bend. This design consisted of 26 U-turns and approximately 2000 1-D apertures.

Microfabrication in PUMA

Chips were microfabricated in polyurethane-methacrylate (PUMA), a transparent non-elastomeric (Shore D60) USP Class VI resin that is UV-curable, as described in previous publications.[27,28] Filtration chips fabricated in PUMA substrate have the advantage that it is optically clear, such that they can be directly placed on a microscope to examine the trapped cells under transmission mode. Also, PUMA is hard enough that tall microstructures (*e.g.* walls forming 1-D apertures) could remain standing without buckling under their own weight or from interfacial adhesion.

A silicon master was first produced using Deep Reactive Ion Etching (DRIE) and subsequently silanized with (tridecafluoro-1,1,2,2-tetrahydrooctyl) trichlorosilane ("TDF-silane") overnight. A polydimethylsiloxane (PDMS) mold was fabricated from this silicon master by pouring degassed PDMS mixture and curing at 75 °C for at least two hours. PUMA resin (Dymax 140-M, Torrington, CT) was dispensed to a 3 mm thickness onto the PDMS mold, and then covered with a transparent cover to prevent oxygen inhibition of the cross-linking reaction. To form fluidic reservoirs or holes for external connection, PTFE posts (3 mm (D) × 3 mm (H)) were embedded in the PUMA resin before curing. The entire assembly was placed in a high-intensity UV source (ADAC Cure Zone 2 UV Flood Light Source, fitted with a 400 W metal halide lamp, providing nominally 80 mW cm^{-2} at 365 nm) for 80 s (exposed through resin side), followed by an additional 40 s (exposed through mold). Once released from the mold, PUMA substrate was conformally bonded to another PUMA-coated (cured) glass coverslip with gentle mechanical pressure. This conformal bond was converted to a permanent bond by placing the PUMA chip under the UV flood source for an additional 10 min.

Cell preparation

Cell culture. MCF-7, a human breast tumor-derived cell line, was from the American Type Culture Collection (ATCC). Cells were maintained in the recommended culture media (EMEM) containing 2 mM L^{-1} glutamine, 10% fetal bovine serum and 50 μg mL^{-1} penicillin/streptomycin at 37 °C with 5% CO_2 in a humidified environment. All cells were seeded at 0.5–1 × 10^4 cells cm^{-2} in a T-75 flask and allowed to grow for 3–5 days until cells reached ~80% confluency. To prepare cell suspensions, adherent cancer cells were treated with 5 mL 0.25% (w/v) trypsin and ethylenediaminetetraacetic acid (EDTA, sodium salt, concentration 2.5 g L^{-1}) for 5 min, diluted with media, and washed (centrifuged at 300 × g for 5 min then resuspended in 5 mL of corresponding diluent). Cells were mixed by vortex or micropipette to obtain uniform suspension and were then adjusted to the desired cell concentration.

Spiking of unfixed cancer cells. Whole human blood, individually drawn from healthy donors, was provided by Plasma International (Everett, WA). Each draw (20 mL) was collected into five Vacutainer tubes containing K_3EDTA anticoagulant,

stored at 4 °C upon arrival, and used within 72 h of the draw. The first tube of each draw was discarded to avoid potential contamination from skin fragments. Cancer cells were siphoned into a TDF-silane-modified glass capillary as described previously[29] and counted manually at least in triplicates under microscope in bright-field. The entire content of the capillary was ejected into a solution of 50 μL whole human blood diluted with 350 μL EMEM. The solution was incubated in phycoerythrin-anti-human Epithelial Cell Adhesion Molecule ("PE-anti-EpCAM") at 1 : 4 (antibody : cell suspension) volume ratio and fluorescein-isothiocyanate-anti-human CD45 ("FITC-anti-CD45") at 1 : 6 ratio for 2 h at room temperature on a rotator, shielded from light. After incubation, the blood solution was flowed through the filtration chip at flow rates of 12.5–16 μL min^{-1}. For the unfixed MCF-7 in media (without human blood), the cells were directly ejected from the capillary into 400 μL EMEM and flowed through the chip.

EpCAM (Epithelial Cell Adhesion Molecule) is present on the cell surface of MCF-7 cancer cells whereas CD45 (also known as leucocyte common antigen) is present only on the surface of leucocytes. To distinguish from non-specific adsorption, a cancer cell must show positive presence of EpCAM but negative of CD45 (EpCAM+/CD45−).

Spiking of fixed cancer cells. To investigate how cell rigidity could affect the retention of cancer cells in filtration, cancer cells were fixed with 4% paraformaldehyde (PFA) for 15 min, washed twice in 1 × PBS, and then resuspended in 1 × PBS to obtain the desired cell concentration. Cells were spiked into 400 μL EMEM using the aforementioned capillary method and flowed through the chip at three different volumetric flow rates. Flow was controlled by regulated compressed air, offering a constant-pressure driving force.

Results & discussion

Importance of flow bypass

Sections below briefly analyze various pressure fields encountered by a cell in a filtration environment (Fig. 2): (1) the hydrodynamic pressure imparted by the carrier fluid as it flows past a cell (Fig. 2(A)); (2) the pressure experienced by a cell occluding a single aperture completely (Fig. 2(B)); and (3) the pressure experienced by a cell occluding an aperture in the presence of multiple parallel apertures available for flow bypass (Fig. 2(C)).

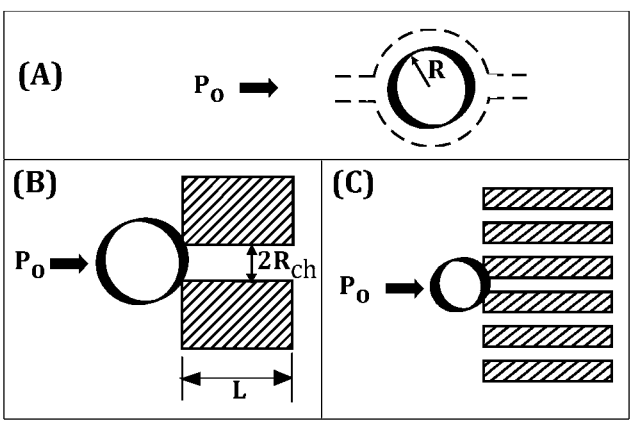

Fig. 2 Various flow configurations that can affect cell pressure: **(A)** shear flow past a spherical cell; **(B)** a cell completely occludes an aperture (0-D); **(C)** a cell completely occludes an aperture in the presence of other unobstructed apertures (0-D).

Scenario 1: Pressure encountered by a single cell in flow. A free particle in flow experiences a pressure differential imparted by the carrier fluid as it flows around the particle (Fig. 2(A)): the upstream half of the particle experiences a higher pressure from the direct impingement of fluid, which leads to a local distribution of pressure around the cell (P) given by:

$$P = P_o + \frac{3}{2}\frac{\mu V}{R}\cos\theta \quad (1)$$

where P_o is the upstream pressure (for convenience, we assumed the downstream pressure to be 0), μ is the viscosity of the carrier fluid, R is the radius of the cell, and V is the relative velocity of the fluid. The angular distribution of the pressure from eqn (1) is plotted in the inset to Fig. 3, with the pressure reaching a maximum at 0° (fluid impinging) and a minimum at 180° (wake). The maximum pressure difference (ΔP_{max}) between 0° and 180° is:

$$\Delta P_{\max} = 3\frac{\mu V}{R} \quad (2)$$

Take a typical value of μ = 1 cps, R = 2.5 μm, and a relative velocity of 1 μm s^{-1}, this pressure differential is on the order of 10^{-3} Pa (or pN μm^{-2}), which is 8 orders of magnitude smaller than an atmosphere.

Scenario 2: A cell occluding a single channel. The pressure experienced by a cell in a filtration environment depends strongly on whether the carrier fluid is able to pass around the cell and

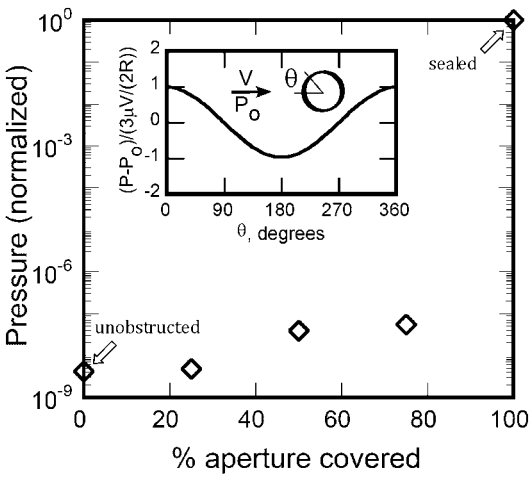

Fig. 3 Cell pressure as a function of the percent area of an aperture blocked. Data points were obtained by solving the Navier–Stokes equation numerically for a 5 μm (D) × 10 μm (L) channel partially blocked by a 5 μm (D) cell, at a fluid velocity of 1 μm s^{-1}. **Inset**: Pressure distribution from a flow around a spherical object. Zero degree is defined as the angle opposite of the upstream flow direction.

equilibrate the pressure. In the case where the cell completely seals a 0-D aperture (Fig. 2(B)), the carrier fluid is unable to recombine behind the cell, and the cell essentially becomes a part of the wall of the main flow channel, experiencing the same pressure that the wall experiences (*i.e.* typically on the order of the externally applied pressure differential to drive the fluid movement in the main flow channel.) The externally applied pressure differential is always larger than the pressure difference from the flow around a cell (*i.e.* as in Scenario 1) by several orders of magnitude, because the former is what is required to drive the flow through the entire filter, and the latter is only a small pressure drop from the fluid wrapping around a cell.

For a partially clogged aperture, some fluid is allowed to pass by the cell and relieve the pressure difference across the cell. The degree of relief is related to the unobstructed cross-sectional area available for flow. Fig. 3 shows the effect on the cell pressure as a cell covers a single 0-D aperture. It is worth noting that even up to 75% obstruction of an aperture, the pressure experienced by a cell at the aperture is still relatively low, within two orders of magnitude of the pressure experienced by a cell in absence of occlusion.

Scenario 3: Occluding in presence of multiple unobstructed parallel channels. In cases where systems of unobstructed parallel channels are available to allow the carrier fluid to bypass and recombine at the exit side of the filtration area (Fig. 2(C)), the pressure experienced by the lodged cell is equivalent to the total pressure drop across the unobstructed parallel channels. For one unobstructed parallel channel, the pressure drop from viscous dissipation (ΔP_{ch}) is given by the Poiseuille equation:

$$\Delta P_{ch} = \frac{32\mu VL}{D_{ch}^{\ 2}} \tag{3}$$

where μ is the viscosity of the carrier fluid, D_{ch} is the hydrodynamic diameter of the channel, L is the length of the channel, and V is the velocity of the fluid.

For n identical parallel channels, the pressure drop is reduced by a factor n, since more cross-sectional area is available for flow:

$$\Delta P_{n-ch} = \frac{32\mu VL}{nD_{ch}^{\ 2}} \tag{4}$$

We can compare this pressure drop to the pressure of a lodged cell at a 1-D aperture (eqn (2)) by making a few simplifying assumptions: if we assume that the length of the channel is at least five times the channel diameter ($L = 5D_{ch}$) and that the diameter of the parallel channels is twice the radius of the lodged cell ($D_{ch} = 2R$) in eqn (4), we arrive at an expression that is similar to eqn (2):

$$\Delta P_{n-ch} = \frac{32\mu V(5(2R))}{n(2R)^2} = \frac{80}{n}\frac{\mu V}{R} \tag{5}$$

Comparing eqn (5) with eqn (2), we note that n, the number of unobstructed bypass channels, must be $\sim 80/3 = 27$; in other words, it takes 27 unobstructed bypass channels to relieve the pressure of one completely sealed aperture. Another way of thinking is that if more than 4% (1/27) of the total apertures are sealed in a 0-D filter, the lodged cells would experience a pressure exceeding that of a cell excluded by a 1-D aperture. This poses a severe capacity issue when 0-D filters are used to isolate cells, namely that most pores must remain unobstructed to avoid building up the pressure.

Increased probability of lysing from multitude of 0-D apertures. The pressure experienced by a cell is directly related to the tension on the cellular membrane: the pressure differential forces the cell to stretch, and when the increase in surface area exceeds 2–4% of the original surface area, the cell is lysed.[30] In a simplified geometry shown in Fig. 4(A), one can relate the pressure required to sustain curvature to the membrane tension according to Laplace's law:

$$\Delta P = 2\tau\left(\frac{1}{R_{ch}} - \frac{1}{R_{out}}\right) \tag{6}$$

where ΔP is the pressure difference between the outside (P_{out}) and the inside (P_{in}) of the channel, R_{ch} is the radius of curvature inside the channel, R_{out} is the radius of curvature of the remaining cell volume outside of the channel, and τ, the membrane tension, is proportional to the surface area change.

In situations where a cell may cover two 0-D apertures simultaneously (Fig. 4(B)), one can analyze the membrane tension by adding up the curvatures:

$$\Delta P_{2-pores} = 2\tau\left(\frac{1}{2R_{ch}} - \frac{1}{R_{out}}\right) \tag{7}$$

where the number of occluded apertures is reflected in the denominator of the first term. Eqn (7) states that for a constant pressure differential, as a cell covers more 0-D apertures (pores),

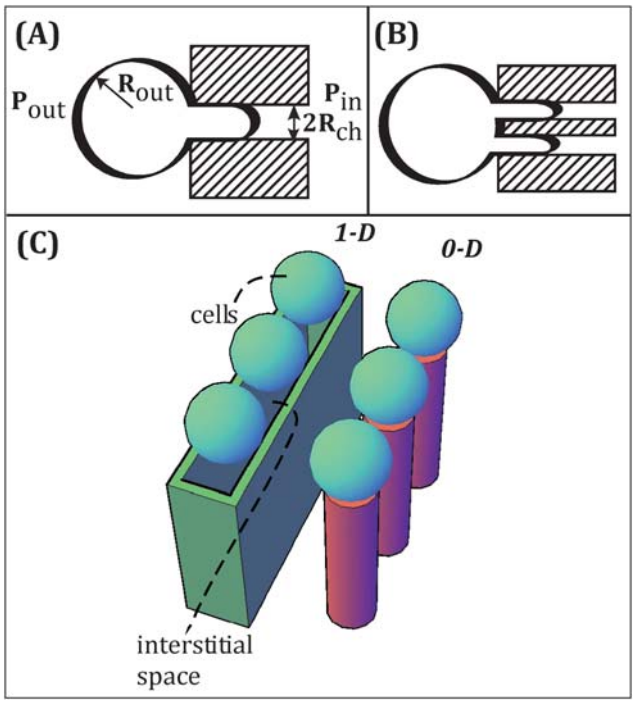

Fig. 4 **(A)** A channel of diameter $2R_{ch}$ completely clogged by a cell with the external radius R_{out}. **(B)** Two channels simultaneously clogged by a cell. **(C)** 1-D aperture *versus* 0-D aperture under high-density cell blockage. 1-D apertures offer interstitial spaces for bypass flow even in close-packing configuration whereas 0-D apertures do not.

the membrane tension τ increases, subjecting the cell to a higher probability of lysis. This is akin to having a cell subjected to patch-clamp aspiration with multiple capillaries: the cell is subjected to multiple points of localized stress on the cell membrane. While mathematically many dots may add up to a line, the key difference between a 1-D aperture and multiple closely packed 0-D apertures, therefore, is the reduction of localized stress which could contribute to cell lysis. Even in situations where a 1-D aperture may trap multiple cells simultaneously, interstitial spaces between close-packed cells are still likely available for fluid flow (Fig. 4(C)). Zero-dimensional apertures do not offer such possibilities.

Application in cancer cell isolation

We tested the ability to isolate cancer cells from fluids using the chips described in the Experimental section. Without adjusting the width of the aperture, the recovery of cancer cells depends on two key parameters: the ability of cells to deform and the velocity at the moment of exclusion.

Fig. 5(A) plots the recovery of cancer cells in the case of cells pre-treated with paraformaldehyde. Paraformaldehyde is commonly used as a cell fixative prior to membrane permeation and fluorescent labeling; in the context of CTC, paraformaldehyde would have been necessary should we choose to screen for the presence of pan-cytokeratin, which is a family of intracellular proteins often targeted for positive confirmation of the epithelial origin of tumor cells. Once cells are fixed, they become rigid, colliding inelastically akin to microbeads. Losing the ability to deform should directly translate to fewer cells lost.

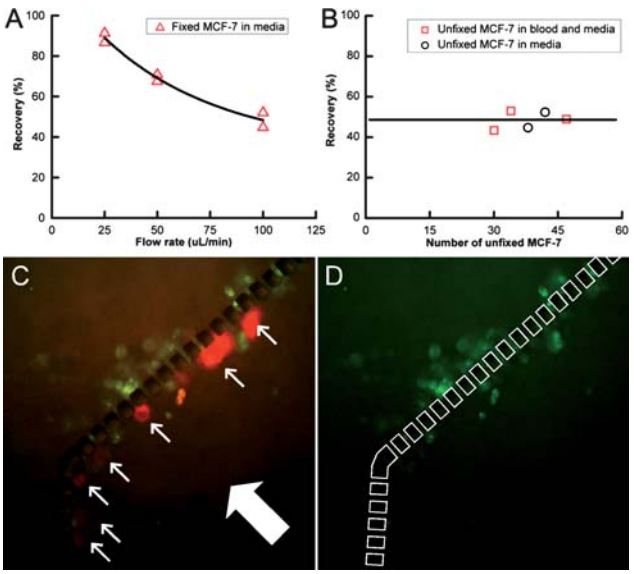

Fig. 5 **(A)** Recovery of PFA-fixed MCF-7 breast cancer cells with 1-D apertures as a function of flow rate. **(B)** Recovery of unfixed MCF-7 breast cancer cells from five runs at 12–16 μL min^{-1}. **(C)** Composite fluorescence image of breast cancer cells (marked by small arrows, with PE-anti-EpCAM re-colored in red) amidst leucocytes (FITC-anti-CD45 in green), isolated from a spiked sample prepared with whole human blood. **(D)** Fluorescence image (with the microfabricated structures outlined for clarity) between 500–540 nm, for identification of leucocytes positively labeled with FITC-anti-CD45.

Indeed Fig. 5(A) shows that the recovery can be as high as 90% at 25 μL min^{-1}; as the flow rate increases up to 100 μL min^{-1}, the recovery decreases to ~50%, suggesting cell loss through the apertures.

Fig. 5(B) plots the recovery of cancer cells in the case of cells not pre-treated with fixative (viable cells). Two sets of recovery data were collected: one set collected with cancer cells suspended in culture media, and a second set collected with cancer cells spiked into whole human blood. The cell mixtures were flowed through the chips at 12–16 μL min^{-1}. The recovery rate was ~50% for unfixed cancer cells at this flow rate, regardless of the suspension the cancer cells were in. Fig. 5(C) shows the composite fluorescent images of cells trapped, where red indicates the binding of PE-anti-EpCAM (EpCAM+) and green indicates the binding of FITC-anti-CD45 (CD45+). Fig. 5(D) shows the FITC-anti-CD45 binding only, for the purpose of identifying the locations of leucocytes. Flow direction is marked by the large white arrow (from lower right corner toward upper left corner). Distinguishable with Fig. 5(C) and 5(D), cells that traversed through the apertures were mostly leucocytes. This can be attributed to the size and deformability differences between leucocytes and cancer cells: the nucleus of cancer cells is typically enlarged with irregular chromatin/nuclear shape.[22,31] So even without fixatives, because cancer cells are larger and less deformable compared to blood cells, they are less likely to traverse through the apertures.

Conclusion

For isolating rare cells, where cell damage could severely compromise the recovery of cells, the forces experienced by cells during the filtration process must be carefully considered. Cells can withstand a certain degree of deformation, but if the membrane area is stretched beyond a few percent, lysis occurs. We showed that by using apertures larger than the cells to be excluded, the force experienced by the excluded cell is, to a large extent, comparable to that in the free flow. When fluid is able to freely flow around the excluded cells, pressure is equilibrated. However, if apertures are smaller than the cells, then the pressure experienced by cells increases and the cells are forced into an extrusion-like environment. For this reason in designing high throughput filtration systems to isolate cancer cells, pores with diameter smaller than cancer cells may cause more damage and lead to cell loss.

We demonstrated that a filtration chip featuring apertures that are nominally larger than a cancer cell is effective in isolating cancer cells from fluids. Cancer cell recovery as high as 90% was achieved, and further design optimization should increase the throughput as well as recovery.

Acknowledgements

We are grateful to Washington State's Life Sciences Discovery Fund (LSDF) for the support of this work.

References

1 A. A. Adams, P. I. Okagbare, J. Feng, M. L. Hupert, D. Patterson, J. Gottert, R. L. McCarley, D. Nikitopoulos, M. C. Murphy and S. A. Soper, *J. Am. Chem. Soc.*, 2008, **130**, 8633–8641.

2 W. J. Allard, J. Matera, M. C. Miller, M. Repollet, M. C. Connelly, C. Rao, A. G. J. Tibbe, J. W. Uhr and L. Terstappen, *Clin. Cancer Res.*, 2004, **10**, 6897–6904.
3 M. Cristofanilli, G. T. Budd, M. J. Ellis, A. Stopeck, J. Matera, M. C. Miller, J. M. Reuben, G. V. Doyle, W. J. Allard, L. Terstappen and D. F. Hayes, *N. Engl. J. Med.*, 2004, **351**, 781–791.
4 S. Nagrath, L. V. Sequist, S. Maheswaran, D. W. Bell, D. Irimia, L. Ulkus, M. R. Smith, E. L. Kwak, S. Digumarthy, A. Muzikansky, P. Ryan, U. J. Balis, R. G. Tompkins, D. A. Haber and M. Toner, *Nature*, 2007, **450**, 1235–U1210.
5 G. Vona, A. Sabile, M. Louha, V. Sitruk, S. Romana, K. Schutze, F. Capron, D. Franco, M. Pazzagli, M. Vekemans, B. Lacour, C. Brechot and P. Paterlini-Brechot, *Am. J. Pathol.*, 2000, **156**, 57–63.
6 L. Zabaglo, M. G. Ormerod, M. Parton, A. Ring, I. E. Smith and M. Dowsett, *Cytometry*, 2003, **55A**, 102–108.
7 S. Zheng, H. Lin, J. Q. Liu, M. Balic, R. Datar, R. J. Cote and Y. C. Tai, *J. Chromatogr., A*, 2007, **1162**, 154–161.
8 V. Zieglschmid, C. Hollmann and O. Bocher, *Crit. Rev. Clin. Lab. Sci.*, 2005, **42**, 155–196.
9 E. Guetta, L. Gutstein-Abo and G. Barkai, *J. Histochem. Cytochem.*, 2005, **53**, 337–339.
10 E. Guetta, M. J. Simchen, K. Mammon-Daviko, D. Gordon, A. Aviram-Goldring, N. Rauchbach and G. Barkai, *Stem Cells Dev.*, 2004, **13**, 93–99.
11 L. Jackson, *Prenatal Diagn.*, 2003, **23**, 837–846.
12 C. B. M. Oudejans, M. L. Tjoa, B. A. Westerman, M. A. M. Mulders, I. J. Van Wijk and J. M. G. Van Vugt, *Prenatal Diagn.*, 2003, **23**, 111–116.
13 M. Schmidt, B. Hoffmann, D. Beelen, A. Gellhaus, E. Winterhager, R. Kimmig and S. Kasimir-Bauer, *Hypertens. Pregnancy*, 2008, **27**, 131–142.
14 G. Vona, C. Beroud, A. Benachi, A. Quenette, J. P. Bonnefont, S. Romana, A. Munnich, M. Vekemans, Y. Dumez, B. Lacour and P. Paterlini-Brechot, *Am. J. Pathol.*, 2002, **160**, 51–58.
15 M. Al-Hajj, M. S. Wicha, A. Benito-Hernandez, S. J. Morrison and M. F. Clarke, *Proc. Natl. Acad. Sci. U. S. A.*, 2003, **100**, 3983–3988.
16 T. Reya, S. J. Morrison, M. F. Clarke and I. L. Weissman, *Nature*, 2001, **414**, 105–111.
17 S. Siena, M. Bregni, B. Brando, N. Belli, F. Ravagnani, L. Gandola, A. C. Stern, P. M. Lansdorp, G. Bonadonna and A. M. Gianni, *Blood*, 1991, **77**, 400–409.
18 J. W. Zhang, C. Niu, L. Ye, H. Y. Huang, X. He, W. G. Tong, J. Ross, J. Haug, T. Johnson, J. Q. Feng, S. Harris, L. M. Wiedemann, Y. Mishina and L. H. Li, *Nature*, 2003, **425**, 836–841.
19 S. H. Seal, *Cancer*, 1964, **17**, 637.
20 R. L. Fleischer, P. B. Price and R. M. Walker, *Science*, 1965, **149**, 383–393.
21 P. Paterlini-Brechot and N. L. Benali, *Cancer Lett.*, 2007, **253**, 180–204.
22 G. Vona, L. Estepa, C. Beroud, D. Damotte, F. Capron, B. Nalpas, A. Mineur, D. Franco, B. Lacour, S. Pol, C. Brechot and P. Paterlini-Brechot, *Hepatology*, 2004, **39**, 792–797.
23 P. Paterlini-Brechot, G. Vona and C. Brechot, *Semin. Cancer Biol.*, 2000, **10**, 241–249.
24 P. Pinzani, B. Salvadori, L. Simi, S. Bianchi, V. Distante, L. Cataliotti, M. Pazzagli and C. Orlando, *Hum. Pathol.*, 2006, **37**, 711–718.
25 H. J. Kahn, A. Presta, L. Y. Yang, J. Blondal, M. Trudeau, L. Lickley, C. Holloway, D. R. McCready, D. Maclean and A. Marks, *Breast Cancer Res. Treat.*, 2004, **86**, 237–247.
26 S. J. Tan, L. Yobas, G. Y. H. Lee, C. N. Ong and C. T. Lim, *Biomed. Microdevices*, 2009, **11**, 883–892.
27 J. S. Kuo, Y. X. Zhao, L. Y. Ng, G. S. Yen, R. M. Lorenz, D. S. W. Lim and D. T. Chiu, *Lab Chip*, 2009, **9**, 1951–1956.
28 J. S. Kuo, L. Y. Ng, G. S. Yen, R. M. Lorenz, P. G. Schiro, J. S. Edgar, Y. X. Zhao, D. S. W. Lim, P. B. Allen, G. D. M. Jeffries and D. T. Chiu, *Lab Chip*, 2009, **9**, 870–876.
29 Y. X. Zhao, P. G. Schiro, J. S. Kuo, L. Y. Ng and D. T. Chiu, *Anal. Chem.*, 2009, **81**, 1285–1290.
30 E. A. Evans, R. Waugh and L. Melnik, *Biophys. J.*, 1976, **16**, 585–595.
31 E. Borgen, B. Naume, J. M. Nesland, G. Kvalheim, K. Beiske, O. Fodstad, I. Diel, E.-F. Solomayer, P. Theocharous, R. C. Coombes, B. M. Smith, E. Wunder, J.-P. Malloleau, J. Garcia and K. Pantel, *Cytotherapy*, 1999, **1**, 377–388.

